

ADA045161

18

19

RADC TR-77-101

9

Final Technical Report - no 2, Jan-Dec 76.

11

March 1977



6

THE MAGNETIC FIELD AND MAGNETIC FIELD GRADIENTS OF THE NUC OCEANOGRAPHIC RESEARCH TOWER.

Physical Dynamics, Incorporated

12 63 p.

Approved for public release; distribution unlimited.

10

George H. Gillespie
Walter N. Podney

14

PD-76-109

Sponsored by
Defense Advanced Research Projects Agency (DoD)
ARPA Order No. 1649

15

F30602-72-C-0494,
ARPA Order-1649

16

1649

17

04

The views and conclusions contained in this document are those of the authors and should not be interpreted as necessarily representing the official policies, either expressed or implied, of the Defense Advanced Research Projects Agency or the U. S. Government.

ROME AIR DEVELOPMENT CENTER
AIR FORCE SYSTEMS COMMAND
GRIFFISS AIR FORCE BASE, NEW YORK 13441

AD No. _____
DDC FILE COPY

408 814

DDC
RECEIVED
OCT 11 1977
B
mt

THE MAGNETIC FIELD AND MAGNETIC FIELD GRADIENTS OF THE
NUC OCEANOGRAPHIC RESEARCH TOWER

George H. Gillespie
Walter N. Podney

Contractor: Physical Dynamics, Incorporated
Contract Number: F30602-72-C-0494
Effective Date of Contract: 1 May 1972
Contract Expiration Date: 31 December 1976
Short Title of Work: The Magnetic Field & Magnetic Field
Gradients of the NUC Oceanographic
Research Tower
Program Code Number: TE20
Period of Work Covered: Jan - Dec 76
Principal Investigator: Dr. Walter Podney
Phone: 703 525-2504
Project Engineer: Joseph J. Simons
Phone: 315 330-4157


Approved for public release; distribution unlimited.

This research was supported by the Defense Advanced
Research Projects Agency of the Department of
Defense and was monitored by Joseph J. Simons (OCS),
Griffiss AFB NY 13441 under Contract F30602-72-C-0494.

This report has been reviewed by the RADC Information Office (OI) and is releasable to the National Technical Information Service (NTIS). At NTIS it will be releasable to the general public including foreign nations.

This report has been reviewed and is approved for publication.

APPROVED:



JOSEPH J. SIMONS
Project Engineer

Do not return this copy. Retain or destroy.

UNCLASSIFIED

SECURITY CLASSIFICATION OF THIS PAGE (When Data Entered)

REPORT DOCUMENTATION PAGE		READ INSTRUCTIONS BEFORE COMPLETING FORM
1. REPORT NUMBER RADC-TR-77-101	2. GOVT ACCESSION NO.	3. RECIPIENT'S CATALOG NUMBER
4. TITLE (and Subtitle) THE MAGNETIC FIELD AND MAGNETIC FIELD GRADIENTS OF THE NUC OCEANOGRAPHIC RESEARCH TOWER		5. TYPE OF REPORT & PERIOD COVERED Final Technical Report #2 Jan - Dec 76
		6. PERFORMING ORG. REPORT NUMBER PD-76-109
7. AUTHOR(s) George H. Gillespie Walter N. Podney		8. CONTRACT OR GRANT NUMBER(s) F30602-72-C-0494
9. PERFORMING ORGANIZATION NAME AND ADDRESS Physical Dynamics, Incorporated P O Box 9271 Arlington VA 22209		10. PROGRAM ELEMENT, PROJECT, TASK AREA & WORK UNIT NUMBERS 62301E 16490402
11. CONTROLLING OFFICE NAME AND ADDRESS Defense Advanced Research Projects Agency 1400 Wilson Blvd Arlington VA 22209		12. REPORT DATE March 1977
14. MONITORING AGENCY NAME & ADDRESS (if different from Controlling Office) Rome Air Development Center (OCS) Griffiss AFB NY 13441		13. NUMBER OF PAGES 52
		15. SECURITY CLASS. (of this report) UNCLASSIFIED
		15a. DECLASSIFICATION/DOWNGRADING SCHEDULE N/A
16. DISTRIBUTION STATEMENT (of this Report) Approved for public release; distribution unlimited.		
17. DISTRIBUTION STATEMENT (of the abstract entered in Block 20, if different from Report) Same		
18. SUPPLEMENTARY NOTES RADC Project Engineer: Joseph J. Simons (OCS)		
19. KEY WORDS (Continue on reverse side if necessary and identify by block number) Magnetic Gradients Gradiometer performance Ocean wave spectra Magnetic Dipole Field		
20. ABSTRACT (Continue on reverse side if necessary and identify by block number) Measurements have been made of the ambient magnetic field and magnetic field gradients near the Naval Undersea Center (NUC) Oceanographic Research Tower. The experiment and its results are summarized in this report. The NUC Tower is located approximately 0.7 miles off the California Coast, near San Diego, and is the proposed site for the shallow water trials of the ARPA Internal Wave Magnetic Sensing (IWMS) experiment. The measurements described here were made in order to accurately determine the magnetic field and associated gradients of (cont on p1473B)		

UNCLASSIFIED

SECURITY CLASSIFICATION OF THIS PAGE(When Data Entered)

A P 1423A)

the NUC tower, so that their significance as a possible source of noise and interference during the IWMS experiment may be assessed. An analytic model of the magnetic field of the NUC tower which accurately describes the field and associated gradients is also described.

4

ACCESSION for		
NTIS	White Section	<input checked="" type="checkbox"/>
DDC	Buff Section	<input type="checkbox"/>
UNANNOUNCED		<input type="checkbox"/>
JUSTIFICATION		
BY		
DISTRIBUTION/AVAILABILITY CODES		
Dist.	and/or	SPECIAL
A		

UNCLASSIFIED

SECURITY CLASSIFICATION OF THIS PAGE(When Data Entered)

Abstract

Measurements have been made of the ambient magnetic field and magnetic field gradients near the Naval Undersea Center (NUC) Oceanographic Research Tower. The experiment and its results are summarized in this report. The NUC Tower is located approximately 7/10 of a mile off the California coast near San Diego, and is the proposed site for the shallow water trials of the ARPA Internal Wave Magnetic Sensing (IWMS) experiment. The measurements described here were made in order to accurately determine the magnetic field and associated gradients of the NUC tower, so that their significance as a possible source of noise and interference during the IWMS experiment may be assessed. An analytic model of the magnetic field of the NUC tower which accurately describes the field and associated gradients is also described.

Table of Contents

Abstract	i
Table of Contents	ii
List of Tables	iii
List of Figures	v
I. Introduction	1
II. Experiment Summary	2
II-1. Magnetic Field Gradient-Measurement Rationale	8
II-2. Experiment Procedure	13
III. Data Analysis and Results for the Magnetic Field and Field Gradients	16
III-1. Instrument Models	16
III-2. Determination of Field Quantities	18
III-3. Determination of Instrument Parameters and Quality of Data Fits	23
IV. Analytic Model of NUC Tower	33
IV-1. Model Description	33
IV-2. Comparison of Model with Measured Data	36
V. Equivalent Dipoles of Measured Gradients	40
VI. Conclusions	47
Acknowledgments	48
References	49
Appendix. Comparison with Previous Measurements	A-1

List of Tables

	<u>Page</u>
Table 1. Coordinates of the points at which magnetic field and field gradient data were obtained. (The x_1 -coordinate in each case is 0.)	15
Table 2. Magnetic field gradients in units of gamma/meter as measured at nine points near the NUC tower. Two measurements of the gradients were made at the A-1 position on March 29 (first set) and March 26 (second set).	21
Table 3. Magnetic field components and total magnetic field in units of gamma as measured at nine points near the NUC tower. Two measurements were made at the A-1 position on March 29 (first set) and March 26 (second set).	22
Table 4. Gradiometer instrument parameters as determined at each of the nine points near the NUC tower where data was collected. Dates of the measurements were: 24 March C-3; 25 March C-2, C-1; 26 March A-1 (second set); 29 March A-3, A-2, A-1 (first set); 30 March B-3, B-2, B-1.	25
Table 5. Magnetometer dc offsets in units of gamma as determined at each of the nine points near the NUC tower where data was collected. \bar{C}_2' is the dc offset of the single axis field output of the gradiometer.	31
Table 6. Standard deviations for the fits to the raw data using the instrument models described in the text.	32
Table 7. Best fit parameters for the field model using a weighted least squares fit to the measured gradient matrix elements.	35

List of Tables (Continued)

	<u>Page</u>
Table 8. Gradient matrix elements in gamma/meter as determined from the best fit model of the NUC tower's magnetic field, and differences between the experimental values and model values.	38
Table 9. Magnetic field components and total field in units of gamma from the best fit model of the NUC tower's magnetic field, and the difference between the experimental values and model values.	39
Table 10. Eigenvalues λ_1 , λ_2 , and λ_3 in units of 100 gamma/m and polar angles of the eigenvector set (\hat{e}_1 , \hat{e}_2 , \hat{e}_3).	42
Table 11. Parameters defining the position vector \underline{r}_1 and equivalent dipole \underline{m}_1 .	43
Table A-1 Magnetic field components and total field in units of gamma as measured at six points near the NUC in January 1975 and the results of the analytic field model. The approximate locations in terms of the positions indicated in figure 1 are shown in parenthesis (position E-4 is a few meters above position E-3). This experimental data is courtesy of Richard Ziemer of Physical Dynamics, Inc., Santa Monica, CA.	A-3

List of Figures

	<u>Page</u>
Figure 1. Geometry of NUC Tower magnetic field and field gradient measurements.	4
Figure 2. Fluxgate magnetometer, gradiometer and turntable mount on a fiberglass boom deployed to the West of the NUC Oceanographic Research Tower. The instruments are shown at the C-3 position indicated in Figure 1.	5
Figure 3. Close-up view from the water of the instrument package deployed at the C-3 position. The turntable is positioned at 0° tilt angle at 0° rotation angle.	6
Figure 4. Close-up view of instrument package from the upper deck of the NUC Tower. The turntable is positioned at 45° tilt angle and 90° rotation angle in this view.	7
Figure 5. Coordinate systems and angles describing the turntable rotations with respect to the NUC Tower.	12
Figure 6. Plots of the raw data (points) and fits (solid curves) for the gradiometer output at the A-1 position. Units are gamma/meter. For each tilt angle, the larger peak-to-peak amplitude curve is for the 26 March measurements, the smaller is for 29 March.	27
Figure 7. Orientation and locations of equivalent dipoles ($\tan 2\alpha = \frac{2}{3} \tan \chi$; for $0 < \alpha < \pi/2$, and $0 < \chi < \pi$).	44
Figure 8. Direction of eigenvectors in the reference frame of the tower.	45
Figure 9. Locations, strengths and orientations of equivalent dipoles for the magnetic gradients determined at each of nine points near the NUC tower.	46

I. Introduction

The Internal Wave Magnetic Sensing (IWMS) experiment will utilize an extremely sensitive superconducting magnetic gradiometer.^{1,2} The successful implementation of that experiment to measure the magnetic field gradients generated by ocean waves³ requires the fielding of the superconducting gradiometer on a suitable platform in an ocean environment. Above surface observations of shallow water internal waves have been proposed to be conducted on the Oceanographic Research Tower of the Naval Undersea Center (NUC) in San Diego, California. The NUC tower is located approximately 7/10 of a mile offshore and has been the site of several internal wave experiments in the past. However, the tower is constructed primarily of ferrous materials and can be expected to significantly alter the earth's magnetic field in its vicinity. The superconducting gradiometer developed for the IWMS experiment has very low noise characteristics in the ambient earth's magnetic field,² but operation in the presence of a disturbed magnetic environment, such as that near the NUC tower, poses a number of problems,¹ which must be addressed for the successful completion of the IWMS experiment. In order to accurately assess the effects of the tower's magnetic environment on the IWMS experiment, measurements were made to determine the magnetic field and magnetic field gradients in the vicinity of the NUC tower.

This report summarizes the concept and execution of the experiment and presents the results for the measured magnetic field and associated gradients. Those results are then used to develop a simple analytic model of the magnetic field near the NUC tower. This model is of sufficient accuracy to use with confidence in the calculation of magnetic field properties in, and near, the region where the experiment was conducted.

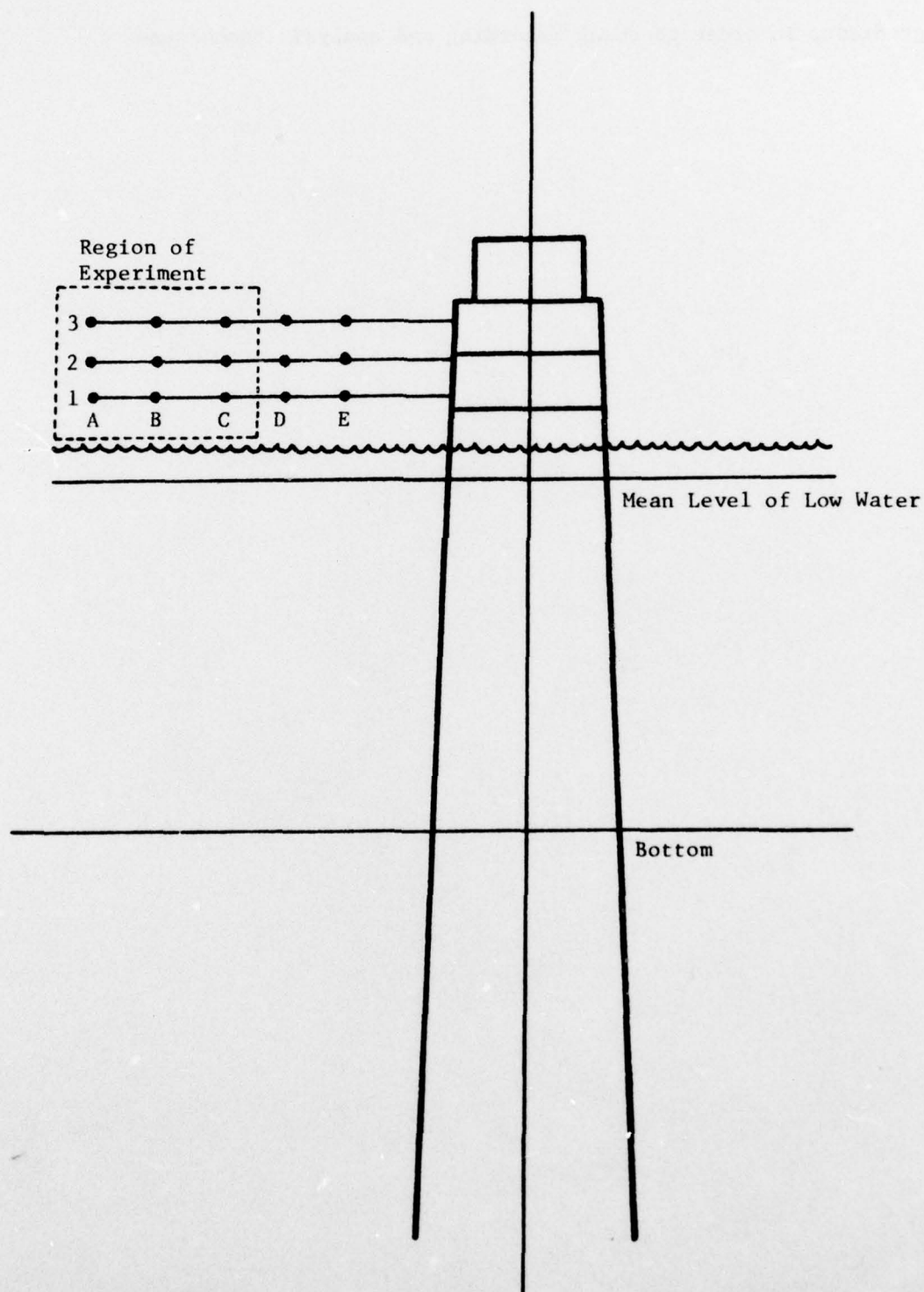
II. Experiment Summary

The objective of the experiment was to measure the components of the steady-state magnetic field and its gradient matrix at selected points near the NUC oceanographic tower. Nine points on the west side of the tower were chosen which span the region where the boom-mounted superconducting gradiometer would be located during the shallow water trials of the IWMS experiment. The locations of these points are indicated schematically in figure 1. To obtain the field information required, a three axis fluxgate magnetometer was used. This directly measures the three orthogonal components of the magnetic field. A single axis fluxgate gradiometer having a longitudinal configuration (coaxial pick-up loops) was used to measure the magnetic field gradients. As will be discussed below, in order to measure all the independent components of the gradient matrix, data must be taken for a number of angular positions of this single axis gradiometer. A special turntable mount was designed and built which allows the gradiometer to be remotely rotated about two axes and locked in position at any of several angles. Figures 2, 3 and 4 show the complete magnetometer, gradiometer and mount deployed at one of the positions during the course of the experiment.

Prior to the experiment on the NUC tower, the magnetometer and gradiometer were calibrated and balanced at a field site at the La Posta Astrogeophysical Observatory, located approximately 70 miles east of San Diego. The calibration coefficients determined there were used throughout the tower experiment. The gradiometer balance was not stable from day to day, so it was redetermined for each measurement point in the data analysis (this is described in Section III). The experiment procedure for

obtaining the required data (described in Section II-2) was also carried out at the La Posta field site using a known magnetic field and field gradient, in order to check recording and analysis techniques.

Figure 1. Geometry of NUC Tower Magnetic Field and Field Gradient Measurements



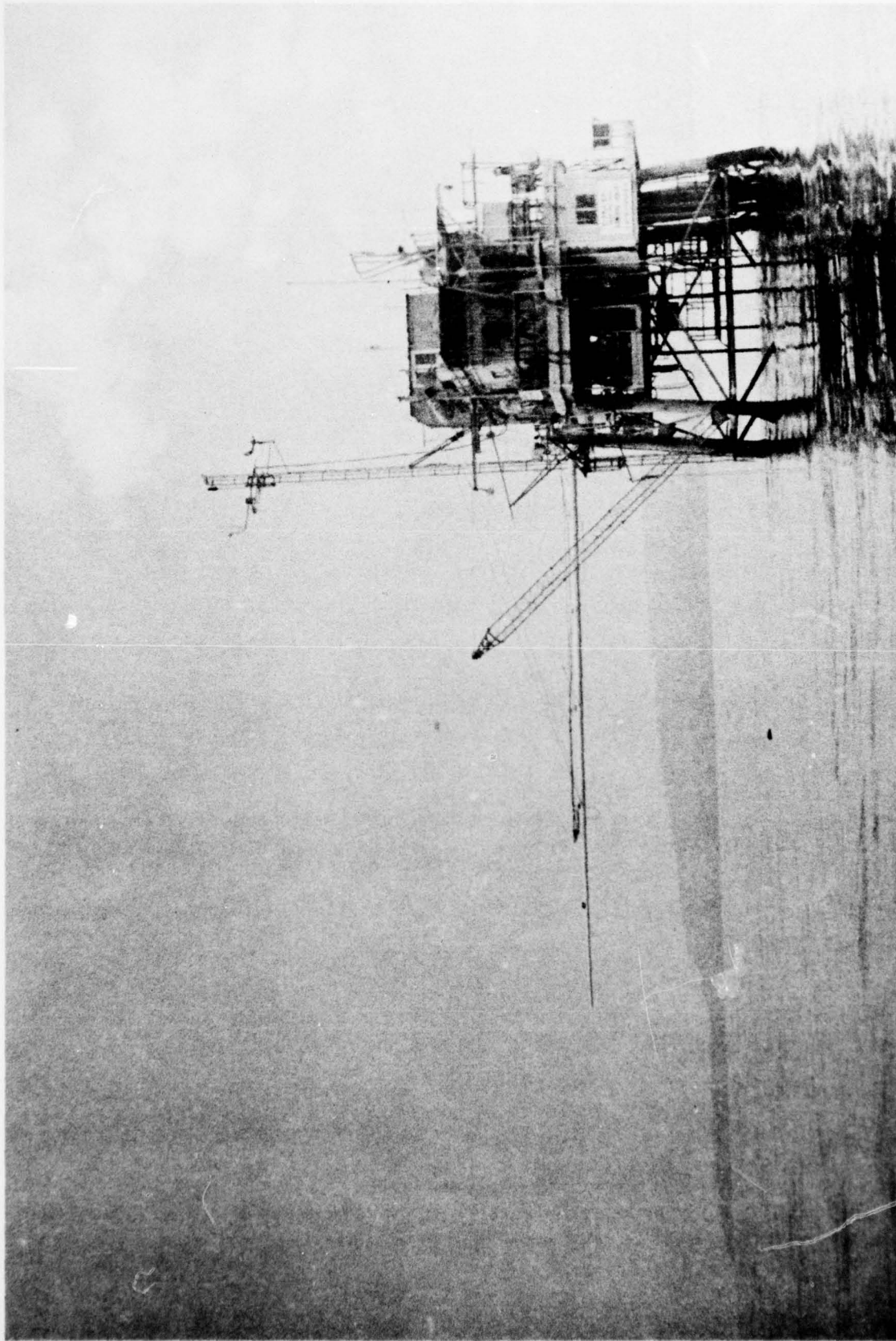


Fig. 2 Fluxgate magnetometer, gradiometer, and turntable mount on a fiberglass boom deployed to the West of the NUC Oceanographic Research Tower. The instruments are shown at the C-3 position indicated in figure 1.

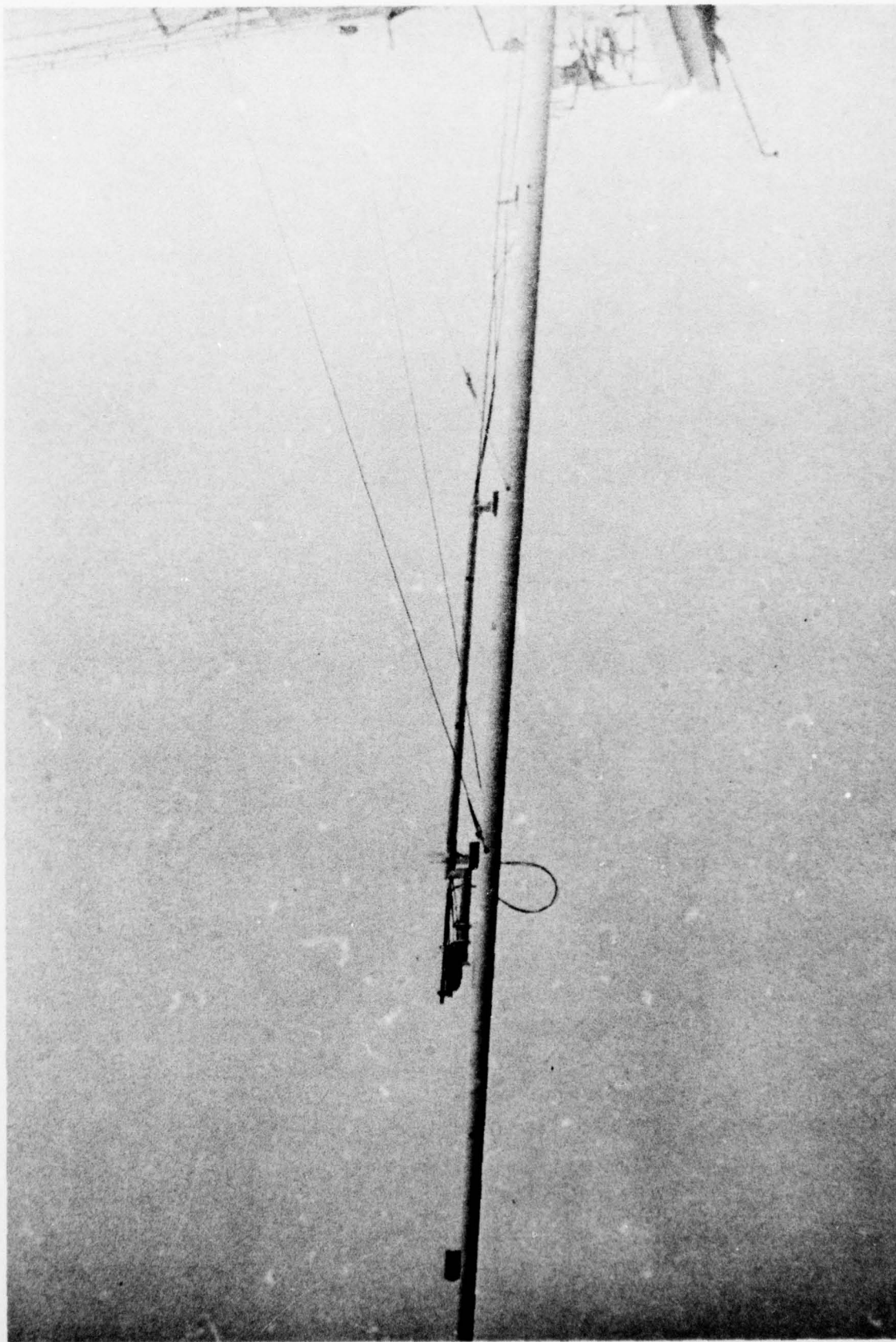


Fig. 3 Close-up view from the water of the instrument package deployed at the C-3 position. The turntable is positioned at 0° tilt angle and 0° rotation angle.

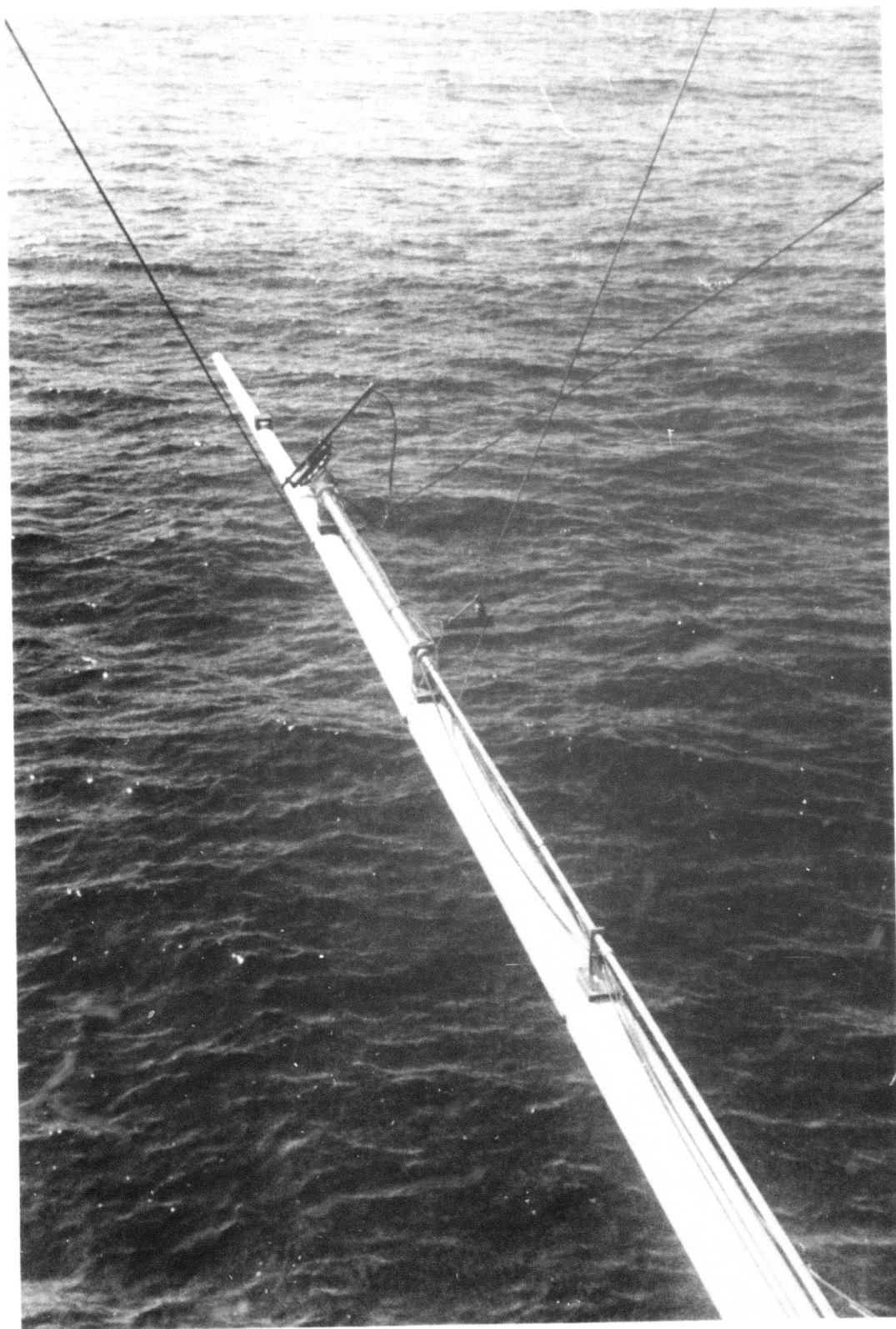


Fig. 4 Close-up view of instrument package from the upper deck of the NUC Tower. The turntable is positioned at 45° tilt angle and 90° rotation angle in this view.

II-1 Magnetic Field Gradient-Measurement Rationale

The gradient of the magnetic field may be written as a second-rank tensor, $\underline{\underline{G}}$. In dyadic notation

$$\underline{\underline{G}} = \underline{\nabla} \underline{B} \quad , \quad (1)$$

where \underline{B} is the magnetic field.

In a particular coordinate system, which is defined by the set of orthogonal unit vectors \hat{x}_i where $i=1,2$ or 3 , the magnetic field may be represented as a 3 component vector and its associated gradient as a 3×3 matrix. The individual elements of the gradient matrix are:

$$G_{ij} = \hat{x}_i \cdot \underline{\underline{G}} \cdot \hat{x}_j = (\hat{x}_i \cdot \underline{\nabla})(\underline{B} \cdot \hat{x}_j) = \frac{\partial}{\partial x_i} B_j \quad . \quad (2)$$

B_j is the component of the magnetic field, \underline{B} , along the \hat{x}_j direction.

From the time-independent Maxwell's equations in free space, both the divergence and curl of \underline{B} are zero,

$$\underline{\nabla} \cdot \underline{B} = 0 \quad , \quad (3)$$

$$\underline{\nabla} \times \underline{B} = 0 \quad . \quad (4)$$

These require that $\underline{\underline{G}}$ be traceless and symmetric, respectively. Consequently, for these conditions there are only 5 independent components of the (3×3) gradient matrix, G_{ij} . In order to determine all five independent components using a single-axis gradiometer, measurements must be made at a number of different angular orientations. The transformation law for rotations of the gradient tensor may then be used to evaluate all the independent components.

Specifically, the gradient tensor, G_{\approx} , transforms under a rotation, described by an operator R , according to

$$G'_{\approx} = R G_{\approx} R^{-1} . \quad (5)$$

Any proper (physical) rotation is equivalent to three successive, independent rotations such as those defined by the Eulerian angles. Consequently the rotation operator R may be written as the product of three separate operators, each only dependent on one of the Eulerian angles. However, for a gradiometer in a longitudinal configuration, only two independent angles are required to specify all the physically distinct orientations of the gradiometer. (The third independent angle may be taken as corresponding to a rotation about the symmetry axis, and the output from an ideal axial gradiometer is invariant under such a rotation.) Therefore, in the following discussion, only two independent rotations will be considered.

In order to provide a simple physical representation basis for the magnetic field, associated gradients, and rotation operators, a fixed coordinate system defined with respect to the NUC tower is used. This coordinate system is indicated in figure 5. The x_3 axis is pointing downward, along the center-line of the tower, the x_2 axis points East, and the x_1 axis points North. The origin is taken to be on the tower center-line, at the ocean floor.

The turntable on which the gradiometer and magnetometer were mounted is capable of rotation about 2 angles, which are also defined in figure 5. The tilt angle, θ , corresponds to a rotation about the x_2 axis in a positive sense, and defines an intermediate coordinate system, with axes labelled as x_1'' , x_2'' , and x_3'' ($x_2'' = x_2$). The rotation angle, ψ , corresponds to a rotation about the x_3'' axis, but in a negative sense. The combination of these two rotations then defines a coordinate system labelled as x_1' , x_2'

and x_3' ($x_3' = x_3''$) which is fixed to the gradiometer and magnetometers.

The corresponding rotation operators, which may be expressed as 3×3 matrices in this representation, are

$$R_{\Theta} = \begin{bmatrix} \cos \Theta & 0 & -\sin \Theta \\ 0 & 1 & 0 \\ \sin \Theta & 0 & \cos \Theta \end{bmatrix}, \quad (6)$$

and

$$R_{\psi} = \begin{bmatrix} \cos \psi & -\sin \psi & 0 \\ \sin \psi & \cos \psi & 0 \\ 0 & 0 & 1 \end{bmatrix}, \quad (7)$$

where

$$R = R_{\psi} R_{\Theta}. \quad (8)$$

The gradiometer was initially aligned ($\Theta = 0$ and $\psi = 0$) such that it measured the G_{22} component of the gradient matrix. Consequently, it measures the G'_{22} component when rotated through the angles Θ and ψ . Evaluating the G'_{22} component of the gradient tensor from equation (5), one finds that the result may be written as:

$$\begin{aligned} G'_{22} &= \hat{x}'_2 \cdot \hat{G} \cdot \hat{x}'_2 \\ &= \frac{1}{2} G_{22} \left[1 + \frac{3}{2} \cos 2\psi + \frac{1}{2} \cos 2\Theta (1 - \cos 2\psi) \right] \\ &\quad + \frac{1}{2} G_{11} \cos 2\Theta (1 - \cos 2\psi) - \frac{1}{2} G_{13} \sin 2\Theta (1 - \cos 2\psi) \\ &\quad + [G_{12} \cos \Theta - G_{23} \sin \Theta] \sin 2\psi. \end{aligned} \quad (9)$$

Equations (3) and (4) have been used in order to reduce the number of gradient matrix elements appearing in (9) to only five independent ones. It is also clear from this result that all five independent elements are required to completely specify the observable G'_{22} for arbitrary angles θ and ψ . Consequently, measurements made at a suitable number of angular orientations allows the determination of the complete gradient matrix in a fixed coordinate system.

II.-2 Experiment Procedure

The single-axis fluxgate gradiometer was mounted on a turntable with the center of rotation for both the angles θ and ψ located at the center of the gradiometer. The three axis fluxgate magnetometer was also mounted on the turntable near the center of rotation. The instruments thus measure the magnetic field and one gradient component effectively at the pivot point of the turntable. In addition, one output of the fluxgate gradiometer provided a single field component measurement, and could be used as a check on one axis of the magnetometer. The entire turntable mechanism could then be attached to any one of several positions on a fiberglass boom which is located on the west side of the NUC tower. The boom may be positioned at different elevations and at different orientations in the East-West vertical plane. The turntable mount was leveled to within about 1 degree during measurements by comparison with the horizon. This procedure was checked with a transit. The x_2 and x_3 coordinates of the pivot point of the turntable could be accurately determined to about 1 or 2 cm, the x_1 coordinate could be estimated to about 10 cm, although the error was probably much less than this. Coordinates of the pivot point for the nine measurement locations (indicated in figure 1) are given in table 1.

The turntable could be remotely oriented (i.e., from the tower deck) at various tilt angles, θ , by turning an aluminum pole which was rigidly attached to the turntable mechanism and supported along the length of the fiberglass boom by several sleeves. The tilt angle could be precisely positioned at values of 0 , $\pm 22\frac{1}{2}^\circ$, and $\pm 45^\circ$ by aligning a brass pin attached to the pole near the turntable with one of five similar pins located on the sleeve nearest the turntable. The error in this alignment was probably no more than 1° . For a fixed tilt angle, full 360° rotations in the angle ψ could

be accomplished from the tower deck by a pulley and cord arrangement. The turntable could be locked at rotation angles of every 15° , with an uncertainty of less than 1° .

Data collection, at each measurement position indicated in figure 1, proceeded as follows. With the turntable fixed at a tilt angle of 0° , data from the gradiometer and each axis of the magnetometer were recorded on a data sheet for each rotation angle of 30° . This data was collected for the full 360° range, including both the 0° and (redundant) 360° positions, and then returned to the 0° rotation angle and the data recorded for this position again. This provided data at 12 distinct rotation angles, with the 0° rotation angle measured 3 different times, providing a check on the repeatability of the measurement procedure. With the turntable returned to the 0° rotation angle, the assembly was turned to the + (or -) $22\frac{1}{2}^{\circ}$ tilt angle position and the data from the outputs recorded for 0° rotation only. The turntable was then turned to the + (or -) 45° tilt position. The data from each instrument was recorded at every 30° rotation angle for the 0° to 360° range, in the same manner as the 0° tilt measurement, including the repeated measurements at 0° rotation angle. With the rotation angle fixed at 0° , the turntable was returned to the + (or -) $22\frac{1}{2}^{\circ}$, and then to 0° tilt position, and the data recorded for those angles, providing additional checks on the repeatability. This procedure was then repeated for values of tilt angles opposite in polarity. This entire measurement sequence provided data at 38 physically distinct angular orientations with multiple measurements at each tilt angle (for the rotation angle fixed at 0°) and required approximately 1 hour to complete for each boom position indicated in figure 1 (after the boom was in position).

Point Label	x_2 (meters)	x_3 (meters)
A-3	-22.20	-25.13
A-2	-22.43	-23.06
A-1	-22.66	-20.92
B-3	-19.20	-25.39
B-2	-19.43	-22.92
B-1	-19.66	-20.71
C-3	-16.20	-25.11
C-2	-16.43	-23.14
C-1	-16.66	-20.79

Table 1. Coordinates of the points at which magnetic field and field gradient data were obtained. (The x_1 -coordinate in each case is 0.)

III. Data Analysis and Results for the Magnetic Field and Field Gradients

III-1 Instrument Models

The output of a perfect gradiometer, as a function of the angles θ and ψ , would be of the form given by equation (9). For a real gradiometer, deviations from the functional form of (9) can be expected. For small differences in the areas or orientations of the gradiometer pick up loops, an imbalance will result between the two fluxgate magnetometers comprising the gradiometer. Additional terms in the output, characteristic of a magnetometer, will then be present. In general, the output of the single-axis gradiometer is a scalar number, and may be written as a sum of scalar products. Specifically:

$$G'_{22} = C'_{22} + \delta' \cdot B + \hat{x}'_2 \cdot G \cdot \hat{x}'_2, \quad (10)$$

where C'_{22} represents any dc offset in the output, δ' is a vector describing the imbalance of the gradiometer, and the last term is the output of a perfect gradiometer. Higher order terms, such as those which could result if the magnetic fields varied significantly over the dimensions of a single pick-up loop in the gradiometer, are assumed to be small.

Equation (10) essentially defines a model of the gradiometer, which is justified only if the data can be adequately described in terms of it. It assumes that the output of the gradiometer can be described in terms of the magnetic field B , the field gradient G and four parameters characteristic of the instrument: the dc offset and the three components of the imbalance vector δ .

An instrument model may also be developed along similar lines for each axis of the fluxgate magnetometer. Effects which were included in the analysis of the magnetometer data essentially correspond to the first two terms appearing

on the right hand side of (10); namely the output of one magnetometer component B'_i , was assumed to be of the form:

$$B'_i = C'_i + \hat{e}(i)' \cdot \underline{\tilde{B}}, \quad (11)$$

where $i = 1, 2$, or 3 . Three instrument parameters, a dc offset C'_i and two components of the unit vector $\hat{e}(i)'$, are required for each axis. The angular dependence of the rotation of the magnetometers is contained in the term $\hat{e}(i)' \cdot \underline{\tilde{B}}$, which may be used to evaluate the components of the magnetic field in the fixed coordinate system. For rotations described by an operator R , the magnetic field transforms as $R\underline{\tilde{B}}$. Consequently, for the specific rotations defined by equations (6) through (8), the term $\hat{e}(i)' \cdot \underline{\tilde{B}}$, may be written as:

$$\begin{aligned} \hat{e}(1)' \cdot \underline{\tilde{B}} &= \epsilon_1(i)' [(B_1 \cos \theta - B_3 \sin \theta) \cos \psi - B_2 \sin \psi] \\ &+ \epsilon_2(i)' [(B_1 \cos \theta - B_3 \sin \theta) \sin \psi + B_2 \cos \psi] \\ &+ \epsilon_3(i)' [B_1 \sin \theta + B_3 \cos \theta] \end{aligned} \quad (12)$$

For an axis of the magnetometer which is perfectly aligned in the primed coordinate system (i.e., is precisely aligned with respect to the axial gradiometer) then $\hat{e}(i)'$ will only have an \hat{x}_i' component. In general, the alignment of the magnetometer with respect to the gradiometer was quite good, and the output of the magnetometer could be adequately described using only the \hat{x}_i' component for $\hat{e}(i)'$. However, previous work had shown that one axis was off in alignment by a few degrees, consequently small contributions from other components were included in the analysis of this axis. The right hand side of equation (12), with the $\hat{e}(i)'$ components replaced by the δ' components of the imbalance vector, also provides the functional form for the imbalance term, $\delta' \cdot \underline{\tilde{B}}$, appearing in equation (10).

III-2 Determination of Field Quantities

In order to determine the five independent elements of the gradient matrix from the data collected as described in section II-2, a Fourier series in the rotation angle ψ was used. The output of the gradiometer was expanded as:

$$G'_{22} = \frac{1}{2} A_0(\theta) + \sum_{n=1}^N [A_n(\theta) \cos(n\psi) + B_n(\theta) \sin(n\psi)] \quad (13)$$

The $2N + 1$ coefficients appearing in (13) were readily calculated using standard Fourier series analysis. Coefficients up to and including $N = 2$ are expected from the angular dependence predicted by equation (10). Equating the coefficients obtained from the data with those arising from the various terms in equation (10) allows one to write a set of equations for the elements of the gradient matrix and the Fourier coefficients at the three tilt angles 0 and $\pm 45^\circ$. The solution to these equations yields the following expressions for the G_{ij} elements:

$$G_{11} = \frac{2}{3} [A_2(45^\circ) + A_2(-45^\circ)] - 2A_2(0^\circ) \quad (14)$$

$$G_{22} = \frac{2}{3} [A_2(45^\circ) + A_2(-45^\circ)] \quad (15)$$

$$G_{12} = \frac{1}{2} B_2(0) + \frac{1}{2\sqrt{2}} [B_2(45^\circ) + B_2(-45^\circ)] \quad (16)$$

$$G_{13} = A_2(-45^\circ) - A_2(45^\circ) \quad (17)$$

$$G_{23} = \frac{1}{\sqrt{2}} [B_2(-45^\circ) - B_2(45^\circ)] \quad (18)$$

The result of this analysis yields the gradient elements, at each of the positions measured, given in table 2. Two sets of gradient elements are given for the position labelled A-1, which were measured on different days with a complete re-positioning of the boom and mount. This gives a measure of the repeatability of the over-all procedure and an estimate of the uncertainty in the results presented. A more complete analysis of the possible errors is contained in section III-3.

A similar approach was used for the calculation of the magnetic field components from the magnetometer data. Again the output of a particular axis, B_1' , was expanded as a Fourier series:

$$B_1' = \frac{1}{2} a_0(\theta) + \sum_{n=1}^N [a_n(\theta) \cos(n\psi) + b_n(\theta) \sin(n\psi)] \quad (19)$$

Equating the coefficients of this expansion with those obtained from equations (11) and (12), a set of equations relating the magnetic field components to the Fourier coefficients is obtained. A set of equations analogous to (14)-(18) results for each axis of the magnetometer, involving a_0 , a_1 , and b_1 at the various tilt angles, θ .

The results of this analysis yielded values for all components of the magnetic field from each axis of the magnetometer (with one exception, which yields only two components of the field), as well as from the single axis magnetometer which comprised part of the gradiometer. In addition, certain axes yield more than one value for a given component. All totalled, this analysis gives seven distinct measurements of the B_1 component, nine measurements of the B_2 component, and four measurements of the B_3 component. These independent determinations were then averaged and the results for each of the nine positions where data was collected are given in Table 3.

It should be pointed out that the identification of the Fourier Series (13) and (19), with terms appearing in the instrument model equations (10) and (11), result in more equations than unknowns. Consequently, the "solutions" are not unique. Additional equations, relating the Fourier coefficients, field quantities and instrument parameters are also obtained. The equations used here were chosen because they require the least information concerning the instrument parameters. The remaining equations not used here are used in the next section to determine the instrument parameters.

Point Label	G_{11}	G_{12}	G_{13}	G_{22}	G_{23}
A-3	-121.14	-51.89	-20.04	335.26	-47.24
A-2	-111.16	-58.61	- 9.62	320.93	-94.22
A-1	-107.51	-48.91	-22.24	286.48	-132.87
	-100.96	-46.38	-18.53	297.12	-141.53
B-3	-226.02	-84.13	- 8.21	527.96	- 30.22
B-2	-224.81	-80.96	-15.63	495.57	-124.89
B-1	-176.94	-82.93	- 4.31	432.80	-210.85
C-3	-378.54	-164.03	-45.38	875.56	- 29.65
C-2	-333.02	-141.13	-22.92	823.10	-204.25
C-1	-301.13	-143.24	-34.31	689.56	-318.31

Table 2: Magnetic field gradients in units of gamma/meter as measured at nine points near the NUC tower. Two measurements of the gradients were made at the A-1 position on March 29 (first set) and March 26 (second set).

Point Label	B_1	B_2	B_3	$ B $
A-3	22,278	7,906	41,150	47,456
A-2	22,223	8,677	40,327	46,855
A-1	22,167 21,928	7,239 7,195	40,630 40,384	46,847 46,513
B-3	21,374	8,892	41,675	47,673
B-2	21,808	8,221	40,800	46,987
B-1	21,237	8,313	40,504	46,483
C-3	21,636	11,032	41,280	47,894
C-2	21,877	10,823	40,588	47,362
C-1	22,094	9,450	39,713	46,417

Table 3. Magnetic field components and total magnetic field in units of gamma as measured at nine points near the NUC tower. Two measurements were made at the A-1 position on March 29 (first set) and March 26 (second set).

III-3 Determination of Instrument Parameters and Quality of Data Fits

The additional equations, relating the Fourier coefficients from (13) and (19) to a combination of field quantities and instrument parameters, were used to calculate values for the instrument parameters. For the gradiometer parameters, the following relations are obtained:

$$C'_{22} = \frac{1}{2\sqrt{2}} \left[A_0(45^\circ) + A_0(-45^\circ) - \sqrt{2} A_0(0) + \frac{1}{\sqrt{2}} G_{11} + \frac{2-\sqrt{2}}{2\sqrt{2}} G_{22} \right] \quad (20)$$

$$\delta'_3 = \begin{cases} \frac{1}{\sqrt{2} B_x} \left[A_0(45^\circ) - A_0(-45^\circ) + G_{13} \right] , \\ \text{or} \\ \frac{1}{B_z} \left[A_0(0) - \frac{1}{2} G_{11} - \frac{1}{2} G_{22} - C'_{22} \right] . \end{cases} \quad (21)$$

$$\delta'_2 = \begin{cases} \frac{A_1(0)B_1 - B_1(0)B_2}{B_1^2 + B_2^2} , \\ \text{or} \\ \frac{A_1(45^\circ) \frac{1}{\sqrt{2}} (B_1 - B_3) - B_1(45^\circ)B_2}{\frac{1}{2}(B_1 - B_3)^2 + B_2^2} , \\ \text{or} \\ \frac{A_1(-45^\circ) \frac{1}{\sqrt{2}} (B_1 + B_3) - B_1(-45^\circ)B_2}{\frac{1}{2}(B_1 + B_3)^2 + B_2^2} . \end{cases} \quad (22)$$

$$\delta'_1 = \begin{cases} \frac{A_1(0)B_2 + B_1(0)B_1}{B_1^2 + B_2^2} , \\ \text{or} \\ \frac{A_1(45^\circ)B_2 + B_1(45^\circ) \frac{1}{\sqrt{2}}(B_1 - B_3)}{\frac{1}{2}(B_1 - B_3)^2 + B_2^2} , \\ \text{or} \\ \frac{A_1(-45^\circ)B_2 + B_1(-45^\circ) \frac{1}{\sqrt{2}}(B_1 + B_3)}{\frac{1}{2}(B_1 + B_3)^2 + B_2^2} . \end{cases} \quad (23)$$

With the magnetic field quantities determined, the instrument parameters could then be calculated from any independent set of 4 of these equations. The remaining equations should then be satisfied, within the experimental error of the data contained on the right-hand side. An optimum set of parameters (and field quantities) could also be determined based on a best fit analysis such as minimizing the χ^2 . For the purposes here, however, a simple average of the instrument parameters determined from all of the equations was performed. Consequently, the dc offset, C'_{22} , was uniquely calculated from (20); the two values of δ'_3 arising from (21) were averaged; and the three values for each of δ'_2 and δ'_1 coming from (22) and (23) were averaged. This yields the parameters given in Table 4 for each of the positions near the NUC Tower where data was collected.

As is clear from the table, the parameters which model the output of the axial gradiometer varied considerably over the course of the experiment. The precise reason for this is not known, but is probably associated with thermal drifts in sensor heads or electronics. The dates on which the measurements were made for each point are indicated in the

Point Label	C'_{22} (gamma/meter)	δ'_1 (meter ⁻¹)	δ'_2 (meter ⁻¹)	δ'_3 (meter ⁻¹)
A-3	12.78	.00004	-.00989	-.00085
A-2	36.45	.00021	-.01023	-.00086
A-1	4.18	-.00005	-.01027	-.00090
	19.50	.00005	-.02182	-.00098
B-3	9.35	.00018	-.02473	-.00065
B-2	0.33	.00024	-.02451	-.00060
B-1	10.46	.00014	-.02479	-.00080
C-3	3.47	-.00006	-.00809	-.00064
C-2	0.73	.00024	-.01324	-.00114
C-1	6.05	.00008	-.01498	-.00115

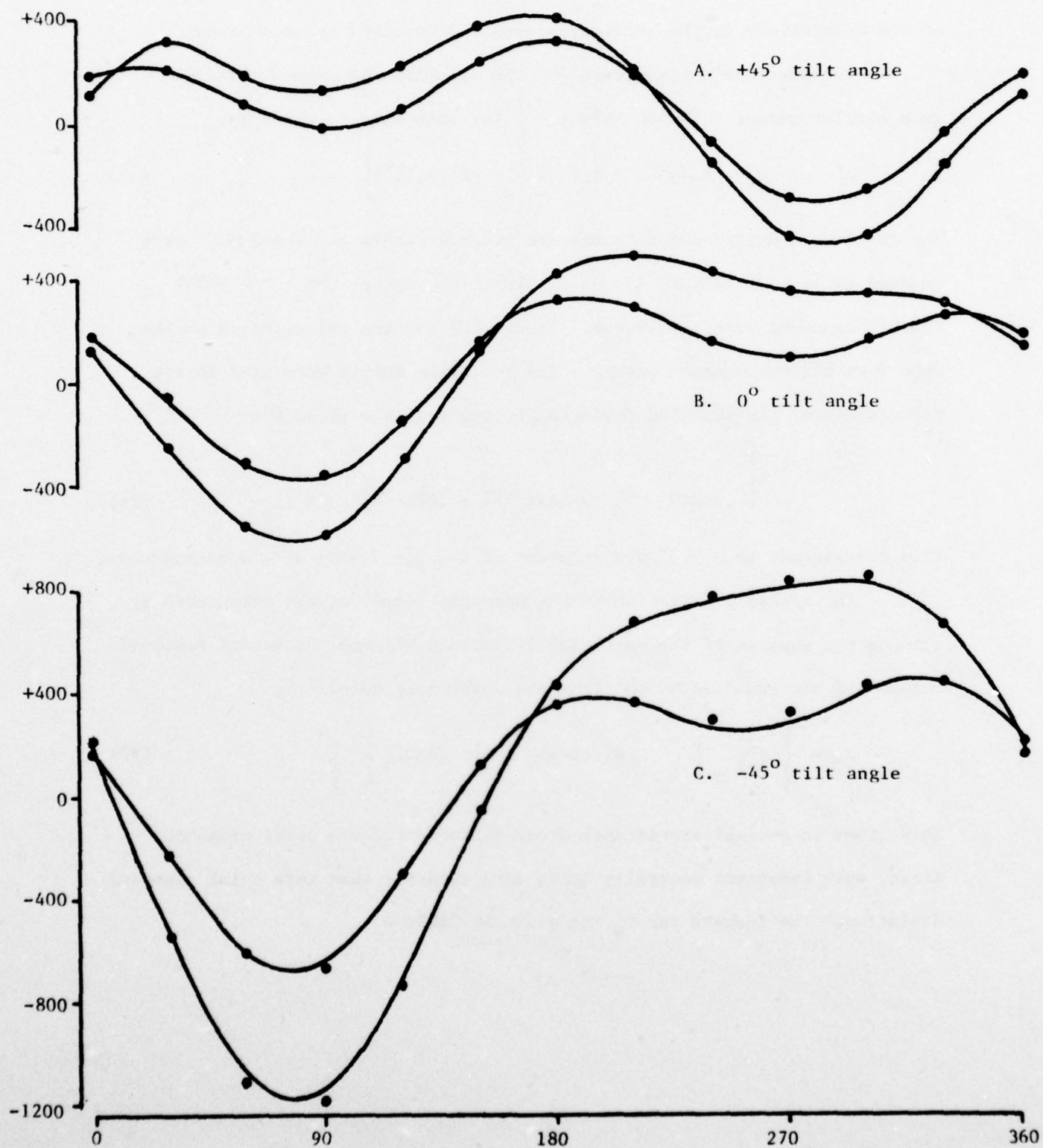
Table 4. Gradiometer instrument parameters as determined at each of the nine points near the NUC Tower where data was collected. Dates of the measurements were: 24 March C-3; 25 March C-2, C-1; 26 March A-1 (second set); 29 March A-3, A-2, A-1 (first set); 30 March B-3, B-2, B-1.

table caption. No systematic effect in the dc offset is apparent, although the sign is always the same. However, while the imbalance vector was relatively constant on a given day, it changed significantly from one day to the next. The size of this effect may be readily estimated from the change in the dominant component, δ'_2 . It varied from about 0.01 to 0.02 (meter⁻¹), indicating that apparent gradients of the order of 500 to 1000 gama/meter could be observed if the gradiometer were aligned parallel to the earth's field. The importance of including these imbalance effects in understanding the output of the gradiometer is also illustrated by a comparison of the data obtained on two different days at the same measurement point. Figure 7 shows the raw data, and the fits based on the gradiometer model described in Section III-1, for the data collected on 26 and 29 March at the A-1 position. The output of the gradiometer is significantly different, several hundred gamma /meter variation at the same angular orientation, although the gradient matrix elements extracted from the analysis (given in Table 2) differ by no more than 9 gamma/meter.

The standard deviations in the fits to the raw data using the functional form of equation (10) were calculated for each of the nine measurement points. With the field quantities from Tables 2 and 3, and the instrument parameters given in Table 4, the expected gradiometer output based on equation (10) was calculated for each angular orientation at which data was collected. Letting $G'_{22}(\text{cal})_\alpha$ represent the actual recorded output for an orientation labelled by α , and $G'_{22}(\text{exp})_\alpha$ represent the actual recorded output for that orientation, then the standard deviation is given by:

$$\sigma_G = \left\{ \frac{1}{N-1} \sum_{\alpha=1}^N \left[G'_{22}(\text{exp})_\alpha - G'_{22}(\text{cal})_\alpha \right]^2 \right\}^{1/2} \quad (24)$$

Figure 6. Plots of the raw data (points) and fits (solid curves) for the gradiometer output at the A-1 position. Units are gamma/meter. For each tilt angle, the larger peak-to-peak amplitude curve is for the 26 March measurements, the smaller is for 29 March.



All 38 physically distinct orientations at which data was recorded were included in calculating the standard deviation for each measurement point. These standard deviations are given in Table 6 and provide an indication of the uncertainty in the gradient elements determined at each point.

The instrument parameters for the magnetometer were determined in a similar manner. The dc offset, C'_i for each axis is given by:

$$C'_i = \frac{1}{2\sqrt{2}} \left[A_0(45^\circ) + A_0(-45^\circ) - \sqrt{2} A_0(0^\circ) \right] . \quad (25)$$

The dc offsets determined this way are given in Table 5. The $\hat{e}(i)'$ were assumed to be unit vectors in the x'_i direction, except for $i = 1$ where three components were calculated. These were average values based on the data from all measurement points. The following values were used in the calculation of the standard deviation to the magnetic field fit:

$$\hat{e}(i)' = \begin{cases} \hat{x}'_i, & i \neq 1; \\ .99845 \hat{x}'_1 - .044 \hat{x}'_2 + .034 \hat{x}'_3, & i = 1. \end{cases} \quad (26)$$

This corresponds to a 3.2° misalignment of the $i = 1$ axis of the magnetometer.

The standard deviation to the magnetic field fit was calculated by summing the squares of the vectorial difference between the actual measured output and the expected output from the instrument model (11):

$$\sigma_B = \left\{ \frac{1}{N-1} \sum_{\alpha=1}^N \left[\tilde{B}'(\text{exp})_\alpha - \tilde{B}'(\text{cal})_\alpha \right]^2 \right\}^{\frac{1}{2}} \quad (27)$$

This gives an overall statistical error estimate for the total magnetic field, each component generally being more accurate than this total standard deviation. The results for σ_B are given in Table 6.

The values for σ_G and σ_B are used in the next section in the development of the analytic field model of the NUC tower. They provide a measure of the relative uncertainty associated with the analysis of the data in terms of the instrument models. However, the standard deviations calculated here only included statistical fluctuations in the data, possible systematic errors such as arise from uncertainties in calibration coefficients have not been included. These effects may result in an overall 10-20% uncertainty in the magnetic field and gradient values given in Tables 2 and 3.

The values for σ_G given in Table 6 indicate that the instrument model for the gradiometer developed in Section III-1 provides a good basis for interpreting the raw data collected during the course of the experiment. Typical uncertainties in the gradient components at the 15-20 gamma/meter level can be expected. The repeat measurement at the A-1 position suggests that it may be even somewhat lower. The errors in a single data point, which may be estimated from the multiple recordings at certain angles as discussed in Section II-2, are typically 5 gamma/meter. The standard deviations in the fits to the data are only modestly larger than this. Barring possible systematic errors, these results indicate that the gradient components given in Table 2 are probably accurate to within about one standard deviation as given in Table 6.

The standard deviations for the magnetic field fits, σ_B , given in Table 6 suggest that uncertainties in the total field measurements may be as large as 700-1100 gamma. The repeat measurement at the A-1 position suggests that actual uncertainties for the magnetic field are

somewhat smaller. The total field difference at the A-1 position measured on two different days was only about 300 gamma. This is the typical variation on the total field observed from the multiple measurements of a single data point as well. These results indicate that the magnetic field data given in Table 3 are probably at least as accurate as the standard deviations given in Table 6, again barring systematic error.

This discussion of the possible errors associated with the determination of the various magnetic field quantities also demonstrates two important aspects of this type of measurement. The uncertainties associated with measuring the magnetic field variation from point-to-point, as indicated by the standard deviations σ_B , are considerably larger than the actual magnetic gradients underlying the variation from point-to-point. This is the reason that a gradiometer, which directly measures spatial variation in the field, was used; rather than trying to extract the variation from an array of magnetometer data alone. Secondly, the use of high statistics allowed a reliable determination of all the field quantities of interest. The collection of data at 38 physically distinct angular orientations, together with the known rotation properties of the gradient matrix, allowed a precise analysis of the data which provided good results for all five independent gradient elements. If data had been collected at only five angular orientations, which in principle should allow the determination of the five independent gradients, the instrument parameters would have been completely indeterminate and several hundred gamma/meter errors would have appeared in the results. The design of the experiment to overdetermine all the field quantities of interest, resulted in much more reliable results than would otherwise have been the case.

Point Label	C'_1	C'_3	C'_2	\bar{C}'_2
A-3	1672	1204	-959	201
A-2	1836	2375	-939	104
A-1	1682	1400	-1003	429
	1677	2382	-1208	-1127
B-3	1891	1106	-1279	-70
B-2	2406	1125	-1125	-304
B-1	1655	1116	-619	429
C-3	1847	924	-817	157
C-2	1514	331	-1418	-228
C-1	1443	885	-711	206

Table 5. Magnetometer dc offsets in units of gamma as determined at each of the nine points near the NUC tower where data was collected. \bar{C}'_2 is the dc offset of the single axis field output of the gradiometer.

Point Label	σ_G (gamma/meter)	σ_B (gamma)
A-3	15	774
A-2	25	916
A-1	15	707
	18	1447
B-3	13	854
B-2	21	1178
B-1	14	660
C-3	12	646
C-2	36	1051
C-1	17	759

Table 6. Standard deviations for the fits to the raw data using the instrument models described in the text.

IV. Analytic Model of NUC Tower

IV-1 Model Description

An analytic model of the magnetic field near the NUC tower was developed in order to provide a simple method for estimating the magnetic field and field gradients at points in and near the region where measurements were made. Three candidate models were considered. One included a uniform (earth's) field contribution and a contribution from a magnetic monopole. The second included an additional monopole, and the third an additional dipole. The third model, consisting of the earth's field, a monopole, and a dipole, provided the best overall fit to the data, and this model is described here. The following definitions are used in this section:

$$\underline{B}_0 = \text{earth's magnetic field, independent of position.} \quad (28)$$

$$\underline{B}_M(\underline{r}) = M \frac{(\underline{r} - \underline{r}_M)}{|\underline{r} - \underline{r}_M|^3} = \text{magnetic field at the position } \underline{r}, \text{ of a magnetic monopole of strength } M \text{ located at } \underline{r}_M. \quad (29)$$

$$\underline{B}_D(\underline{r}) = \frac{3(\underline{r} - \underline{r}_D)(\underline{r} - \underline{r}_D) \cdot \underline{D}}{|\underline{r} - \underline{r}_D|^5} - \frac{\underline{D}}{|\underline{r} - \underline{r}_D|^3}$$

= magnetic field at the position \underline{r} , of a magnetic dipole of dipole moment \underline{D} located at \underline{r}_D . (30)

The field model is simply the sum of these three contributions. The matrix elements, G_{ij} , resulting from the model are:

$$\begin{aligned}
G_{ij} = & M \frac{1}{|\underline{r}-\underline{r}_M|^3} \left\{ \delta_{ij} - 3 \frac{(\underline{r}-\underline{r}_M) \cdot \hat{x}_i (\underline{r}-\underline{r}_M) \cdot \hat{x}_j}{|\underline{r}-\underline{r}_M|^2} \right\} \\
& + \frac{3}{|\underline{r}-\underline{r}_D|^4} \left\{ \left[\delta_{ij} - 5 \frac{(\underline{r}-\underline{r}_D) \cdot \hat{x}_i (\underline{r}-\underline{r}_D) \cdot \hat{x}_j}{|\underline{r}-\underline{r}_D|^2} \right] \frac{(\underline{r}-\underline{r}_D) \cdot \underline{D}}{|\underline{r}-\underline{r}_D|} \right. \\
& \left. + \frac{(\underline{r}-\underline{r}_D)_i D_j + (\underline{r}-\underline{r}_D)_j D_i}{|\underline{r}-\underline{r}_D|} \right\}. \quad (31)
\end{aligned}$$

The four parameters of the monopole, M and \underline{r}_M , and the six parameters of the dipole, \underline{D} and \underline{r}_D , were determined by a least squares fit to the gradient elements given in Table 2. Each point was weighted according to the standard deviations given in Table 6. Specifically,

$$\left(\frac{\Delta G}{\sigma_G} \right)^2 = \left[\frac{G_{ij} \text{ (Equation 31)} - G_{ij} \text{ (exp)}}{\sigma_G \text{ (exp)}} \right]^2, \quad (32)$$

was summed over the 9 positions and 5 independent elements and a search over the 10 parameters was made to minimize this χ^2 . The best fit parameters determined in this manner are given in Table 7.

With the monopole and dipole contributions to the field model determined, the earth's field components were adjusted to obtain a best fit to the magnetic field data given in Table 3. Again a χ^2 function using the standard deviation of the field data (σ_B from Table 6) was minimized. The earth's field so determined is:

$$\underline{B}_0 = [22,161 \hat{x}_1 + 3,912 \hat{x}_2 + 41,491 \hat{x}_3] \text{ gamma} \quad (33)$$

Monopole Parameters

$$M = - \frac{1}{4\pi} [2.14 \times 10^7] \text{ gamma-meter}^2$$

$$\underline{r}_M = [5.13 \hat{x}_1 - 0.59 \hat{x}_2 - 26.09 \hat{x}_3] \text{ meters}$$

Dipole Parameters

$$\underline{D} = \frac{1}{4\pi} [1.06 \times 10^8 \hat{x}_1 + 3.13 \times 10^7 \hat{x}_2 - 7.6 \times 10^3 \hat{x}_3] \text{ gamma-meter}^3$$

$$\underline{r}_D = [-0.36 \hat{x}_1 - 1.18 \hat{x}_2 - 23.90 \hat{x}_3] \text{ meters}$$

Table 7. Best fit parameters for the field model using a weighted least squares fit to the measured gradient matrix elements.

IV-2. Comparison of Model with Measured Data

The magnetic field gradient elements calculated at each of the nine measurement positions are given in Table 8. Below each entry is the difference between the experimental value and the field model value. Table 9 gives the same information for the magnetic field components.

The results presented in Table 8 show that the bulk of the features exhibited by the measured data are reproduced by the field model described here. Both the monopole and dipole term play an important role in the model. For example, all of the signs of the off-diagonal gradient elements cannot be reproduced by a monopole model alone. If the dipole moment is set to zero, the signs of all the G_{12} elements are positive, in clear contradiction with the measured data. The differences between the measured data and the values calculated from the model are not always within the one standard deviation uncertainty. Gradient differences of the order of $3\sigma_G$ are apparent. This is not too surprising, however. The NUC Tower is a very complicated structure; simple models of the field could only be expected to reproduce most of the gross features. However, most of the larger discrepancies are associated with the larger elements, so that as a percentage the errors in the model predictions are not expected to be very large.

The results of the model for the magnetic field components given in Table 9 also reproduces all of the bulk features. This provides a self-consistency check on the field model and provides confidence that no large systematic effects have been overlooked.

The overall (uncorrelated) χ^2 for the gradient matrix fit is 85 (45 data points, 10 parameter fit). For the magnetic field fit, the χ^2 is 10 (15 data points, 3 parameter fit). These are respectable fits. A comparison with previous data taken at the NUC tower and also with other information on the earth's magnetic field near San Diego is presented in the Appendix.

Point Label	G_{11}	G_{12}	G_{13}	G_{22}	G_{23}
A-3	-161.15 (40.01)	-27.03 (-24.86)	-12.34 (-7.70)	350.09 (-14.83)	-11.35 (-35.89)
A-2	-153.98 (42.82)	-30.02 (-28.59)	-8.32 (-1.30)	326.71 (-5.78)	-62.14 (-32.08)
A-1	-143.22 (35.71)	-30.40 (-18.51)	-3.83 (-18.41)	287.07 (-0.59)	-102.66 (-30.21)
B-3	-241.00 (14.98)	-60.38 (-23.75)	-26.88 (18.67)	538.53 (-10.57)	-3.95 (-26.27)
B-2	-228.32 (3.51)	-68.97 (-11.99)	-14.85 (-0.78)	492.37 (3.20)	-113.70 (-11.19)
B-1	-208.25 (31.31)	-67.15 (-15.78)	-3.39 (-1.15)	412.84 (19.96)	-181.92 (-28.93)
C-3	-377.52 (-1.02)	-163.89 (-0.13)	-61.74 (16.36)	881.71 (-6.15)	-23.41 (-6.24)
C-2	-357.15 (24.13)	-177.00 (35.87)	-31.73 (8.81)	800.17 (22.93)	-196.52 (-7.73)
C-1	-318.41 (17.28)	-165.40 (22.16)	2.57 (-36.88)	629.77 (59.79)	-331.47 (13.16)

Table 8. Gradient matrix elements in gamma/meter as determined from the best fit model of the NUC tower's magnetic field, and differences between the experimental values and model values.

Point Label	B_1	B_2	B_3	$ B $
A-3	22,037 (241)	7,740 (166)	41,386 (-236)	47,522 (-66)
A-2	22,022 (201)	7,584 (1,093)	41,018 (-691)	47,170 (-315)
A-1	22,016 (151)	7,334 (-95)	40,696 (-66)	46,847 (0)
B-3	21,918 (-544)	9,049 (-157)	41,422 (253)	47,729 (-56)
B-2	21,881 (-73)	8,779 (-558)	40,733 (67)	47,064 (-77)
B-1	21,877 (-640)	8,342 (-29)	40,247 (257)	46,562 (-79)
C-3	21,601 (35)	11,114 (-82)	41,277 (3)	47,895 (-1)
C-2	21,547 (330)	10,696 (127)	40,359 (229)	46,984 (378)
C-1	21,555 (539)	9,892 (-442)	39,527 (186)	46,096 (321)

Table 9. Magnetic field components and total field in units of gamma from the best fit model of the NUC tower's magnetic field, and the difference between the experimental values and model values.

V. Equivalent Dipoles of Measured Gradients

Because a steady magnetic field in free space is both nondivergent and irrotational, its gradients at a point in free space are equivalent to the gradient field of a magnetic dipole located on a sphere of unit radius about the point. As we describe elsewhere¹, we find the orientation and location of an equivalent dipole by requiring eigenvalues and principal axes of its gradient field to be respectively equal to and coincident with eigenvalues and principal values of gradients at the field point. Because the sense of an eigenvector defining direction along a principal axis is indeterminant, the four sets of eigenvectors $(\hat{e}_1, \hat{e}_2, \hat{e}_3)$, $(-\hat{e}_1, \hat{e}_2, -\hat{e}_3)$, $(-\hat{e}_1, -\hat{e}_2, \hat{e}_3)$ and $(\hat{e}_1, -\hat{e}_2, -\hat{e}_3)$ define the same principal axes and so correspond to the same set of eigenvalues $(\lambda_1, \lambda_2, \lambda_3)$. As a result, each of four dipoles located on a sphere of unit radius about a field point give the same gradients at the field point.

Figure 7 shows orientation and location of a dipole m_1 that produces a gradient field whose eigenvalues are λ_1, λ_2 , and λ_3 , and whose principal axes coincide with the set of eigenvectors $(\hat{e}_1, \hat{e}_2, \hat{e}_3)$. The dipole axis and position vector r_1 lie in the plane normal to the eigenvector position \hat{e}_2 . Dashed lines in Figure 7 delineate orientation and location of dipoles that produce gradient fields, having eigenvalues λ_1, λ_2 , and λ_3 , whose principal axes coincide with the sets of eigenvectors $(\hat{e}_1, -\hat{e}_2, -\hat{e}_3)$, $(-\hat{e}_1, \hat{e}_2, -\hat{e}_3)$, and $(-\hat{e}_1, -\hat{e}_2, \hat{e}_3)$ as noted. As is evident, the four equivalent dipoles lie in the plane normal to the eigenvector \hat{e}_2 , and they form the two pairs $(m_1, r_1; -m_1, -r_1)$ and $(m_2, r_2; -m_2, -r_2)$. The relation

$$\tan \chi = \frac{|\lambda_1 \lambda_3|^{1/2}}{\lambda_2}, \quad 0 < \chi < \pi$$

determines the angle χ between the dipole axis and position vector of an equivalent dipole, and the relation

$$g = \frac{\mu_o 3m}{4\pi r^4} = |\lambda_2^2 + \lambda_1 \lambda_3|^{1/2}$$

gives magnitude of its dipole moment.

Table 10 lists the eigenvalues* and polar angles defining directions of the set of eigenvectors $(\hat{e}_1, \hat{e}_2, \hat{e}_3)$ for each measurement position. Figure 8 shows directions of the set of eigenvectors $(\hat{e}_1, \hat{e}_2, \hat{e}_3)$ in the frame of reference $\{\hat{x}_i\}$ used to define measured gradient elements. The principal axis corresponding to eigenvalue λ_1 is approximately aligned with the horizontal \hat{x}_2 axis; the principal axis corresponding to eigenvalue λ_2 , with the horizontal \hat{x}_1 axis; and the principal axis corresponding to eigenvalue λ_3 , with the vertical \hat{x}_3 axis. The plane containing axes of equivalent dipoles is nearly vertical with \hat{x}_3 axis. The plane containing axes of equivalent dipoles is nearly vertical with its normal vector \hat{e}_2 facing north.

Table 11 lists dipole strengths and polar angles defining the directions of the position vector \underline{r}_1 , and of the dipole axis of the equivalent dipole \underline{m}_1 located on a sphere of unit radius about each measurement position. Figure 9 depicts locations and orientation of the equivalent dipole \underline{m}_1 in the vertical plane containing measurement positions. Lengths of dipole vectors are drawn in proportion to their strength.

* Eigenvalues are indexed so that $\lambda_1 > \lambda_2 > \lambda_3$.

Position	λ_1	λ_2	λ_3	ϕ_1	Θ_2	ϕ_2	Θ_2	ϕ_3	Θ_3
A-3	3.45	-1.21	-2.24	276.2	85.4	4.6	104.4	23.4	15.2
A-2	3.44	-1.15	-2.29	277.1	80.5	5.3	100.9	47.3	14.5
A-1	3.26	-1.01	-2.24	275.7	75.6	1.0	107.6	42.9	23.1
B-3	5.38	-2.33	-3.05	276.3	88	5.9	99.4	18.1	9.6
B-2	5.24	-2.22	-3.02	276	81.2	2.3	112.7	25.8	24.5
B-1	5.01	-1.81	-3.21	276.9	74.6	3.3	102.6	55.7	20.1
C-3	8.97	-3.8	-5.18	277.3	89	6.9	112.5	9.6	22.5
C-2	8.7	-3.38	-5.32	276.5	81.6	4.4	104.2	36.2	16.6
C-1	7.92	-2.90	-5.02	277	75.2	0.9	111.8	38.5	26.8

Table 10. Eigenvalues λ_1 , λ_2 , and λ_3 in units of 100 gamma/m and polar angles of the eigenvector set (\hat{e}_1 , \hat{e}_2 , \hat{e}_3).

Position	m/r^4 , amp/m ²	χ	α	ϕ_{r_1}	\odot_{r_1}	ϕ_{m_1}	\odot_{m_1}
A-3	0.83	118.9	64.8	89.4	70.3	215.8	163.3
A-2	0.85	116.7	63.5	92	73.5	227.9	165.4
A-1	0.84	113.8	61.7	87	77.5	212.9	159.6
B-3	1.11	134.7	73	93.5	75.2	260	149
B-2	1.1	132.3	71.9	89	82	242.2	140.2
B-1	1.19	120.4	65.7	91.5	81.7	244.8	154.9
C-3	1.89	132.2	71.8	90.2	74.2	237.6	146.8
C-2	1.97	124.9	68.2	91.1	77.2	242.8	154.2
C-1	1.87	121.2	66.1	88	82.7	230.1	148.5

Table 11. Parameters defining the position vector \underline{r}_1 and the equivalent dipole \underline{m}_1 .

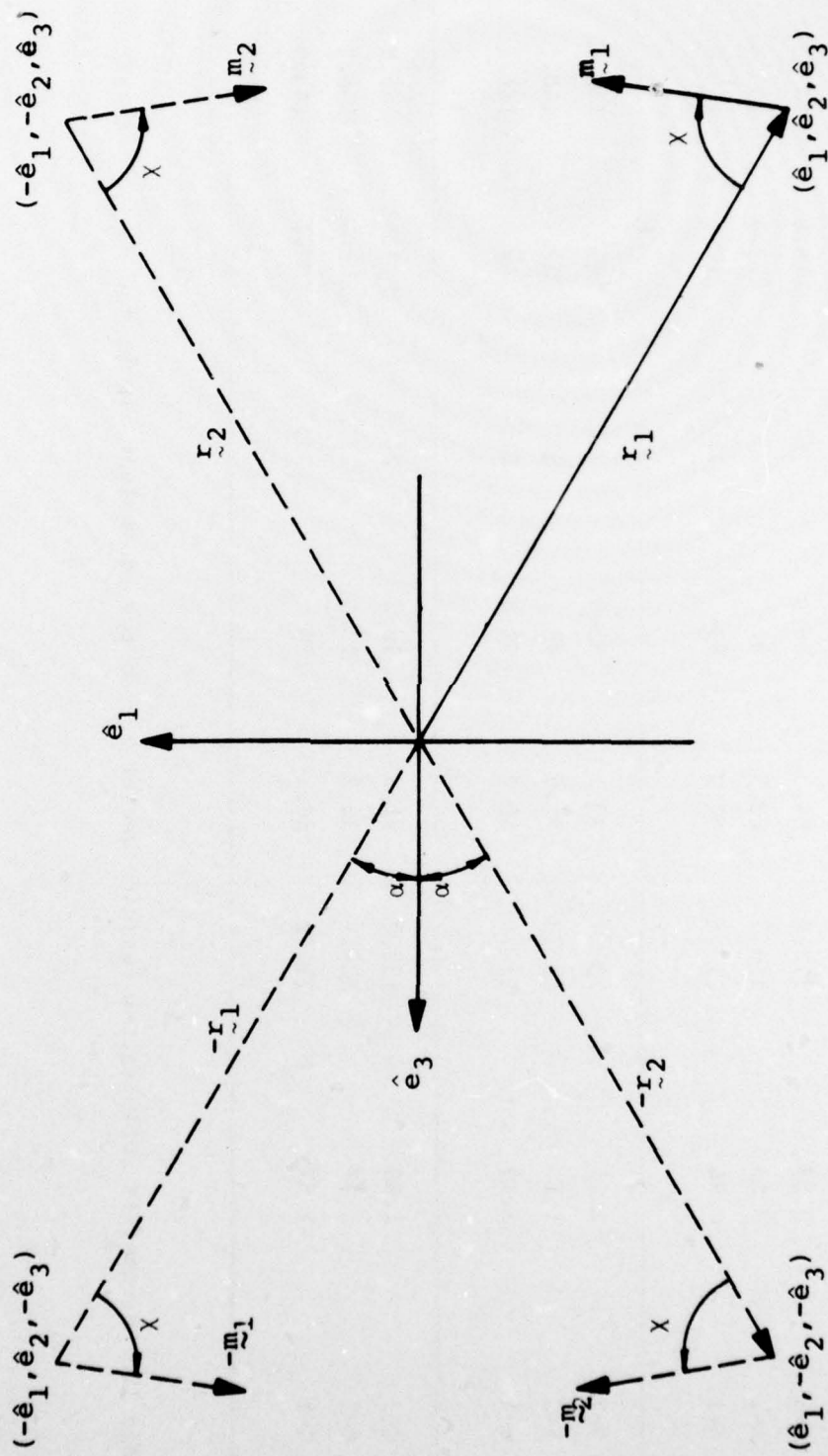


Figure 7. Orientation and locations of equivalent dipoles ($\tan 2\alpha = 2/3 \tan \chi$; for $0 < \alpha < \pi/2$, and $0 < \chi < \pi$).

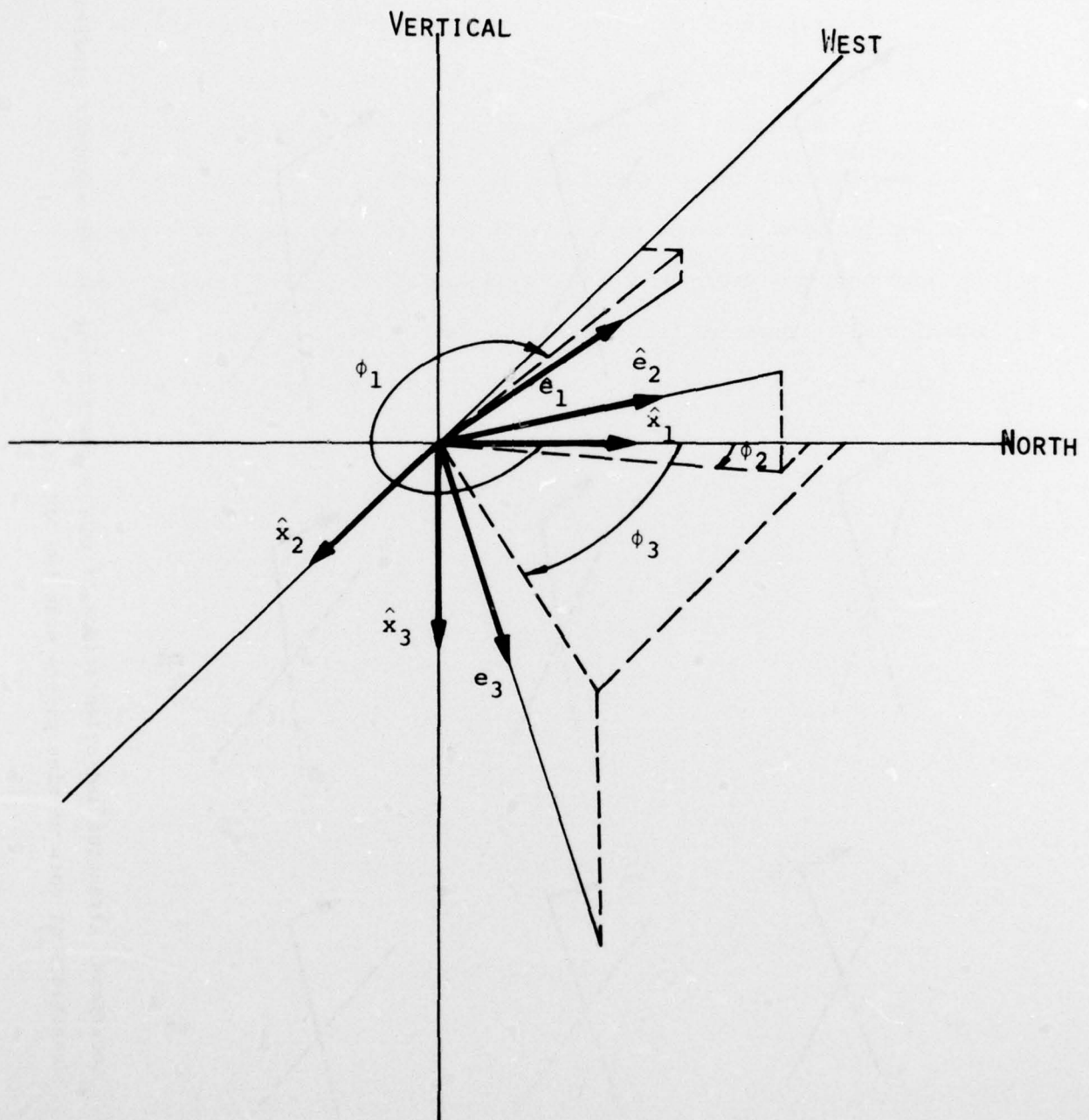


Figure 8. Direction of eigenvectors in the reference frame of the tower.

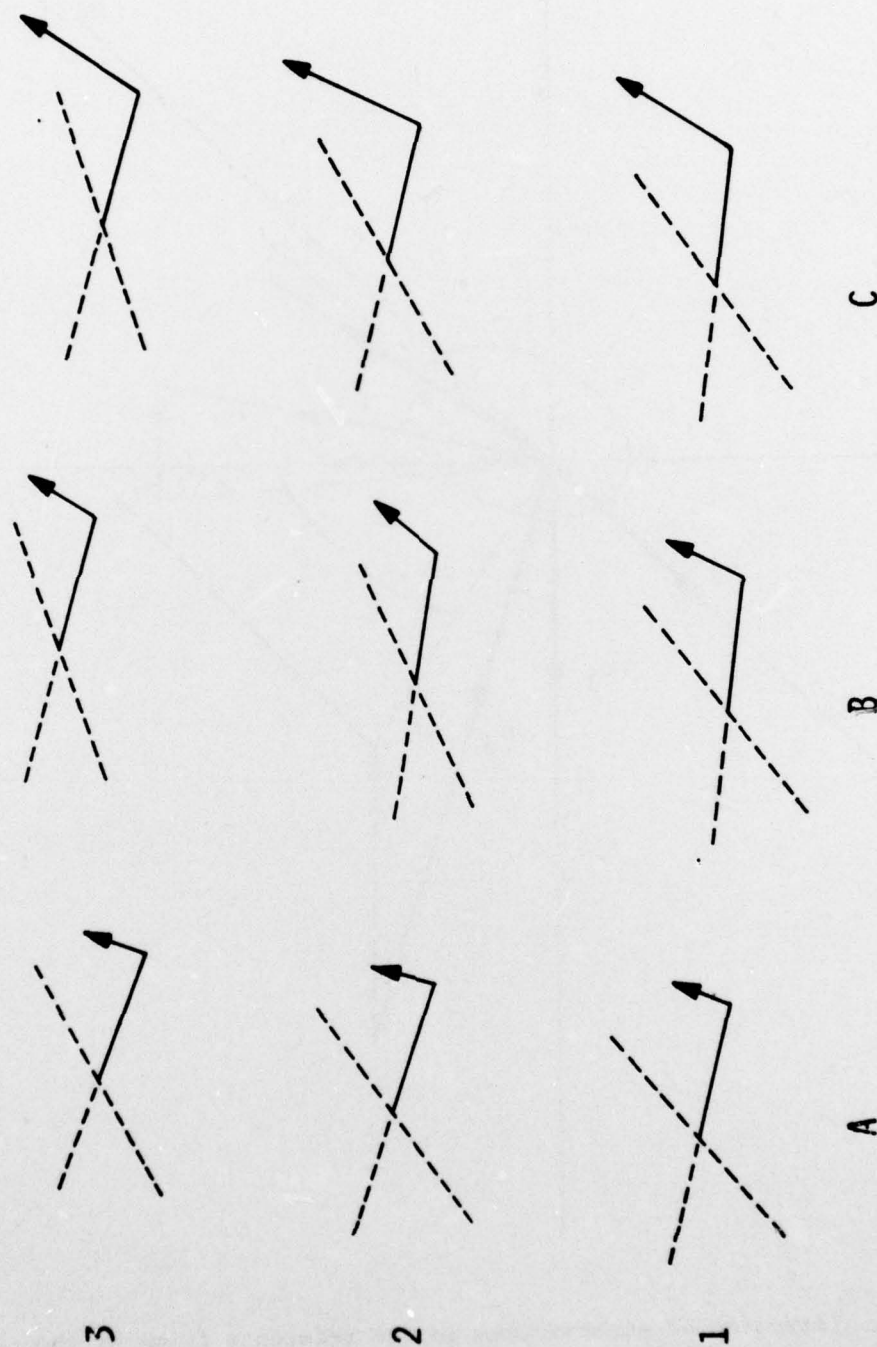


Figure 9. Locations, strengths and orientations of equivalent dipoles for the magnetic gradients determined at each of nine points near the NUC tower.

VI. Conclusion

The experiment described in this report provided a precise measurement of the magnetic field and associated magnetic field gradients at selected points in a region to the west of the NUC Oceanographic Research Tower. The results of those measurements provide a reliable data basis on which to examine interference and noise effects for the proposed Internal Wave Magnetic Sensing Experiment. An analytic model of the NUC Tower's magnetic field was constructed which reproduces the important features of the data. This model may be used for estimating the magnetic field and associated gradients in, and near, the region in which data was collected.

Acknowledgements

The authors are indebted to the Ocean Measurements Group of the Naval Undersea Center, under the direction of Dale Good, for their invaluable support in carrying out most of the field work required for this experiment. The assistance of Jim Buxton is greatly appreciated in conducting the land based testing and calibrations at the La Posta Astrogeophysical Observatory; and the assistance of the Observatory staff, headed by Max Bleiweiss, is also highly appreciated. Ralph Janda's effort in developing the programs for the computational parts of this work is gratefully acknowledged. This work was supported by the Defense Research Advanced Projects Agency and was monitored by the Rome Air Development Center under contract F30602-72-C-0494.

REFERENCES

1. W. Podney and G. Gillespie, "Measurement of Ambient Magnetic Field Gradients Using a Superconducting Magnetic Gradiometer," Physical Dynamics, Inc. Report No. PD-76-107, in preparation (1976).
2. G. Gillespie, W. Podney and J. Buxton, "Low Frequency Noise Spectra of a Superconducting Magnetic Gradiometer," Physical Dynamics, Inc. Technical Memorandum, to be published in Journal of Applied Physics, (1976).
3. W. Podney, "Electromagnetic Fields Generated by Ocean Waves," J. Geophys. Res. 80, 2977 (1975).

APPENDIX A

Comparison with Previous Measurements

A previous survey of the magnetic field near the NUC tower, in a region which partially overlaps that examined by this report, was conducted in January 1975 and is described in another report (Physical Dynamics, Inc. report PD-SM-76-112, Appendix A, 1976). Data were collected in that experiment using a three axis fluxgate magnetometer similar to that utilized in the work described in this report. No gradiometer or angular rotation data were collected in the earlier survey. The results of those measurements, together with the field values predicted by the analytic model of NUC tower's magnetic field described in Section IV of this report, are given in Table A-1.

The results presented in the table indicate that the overall features of the data are approximately described by the analytic field model (e.g., the trend of B_2 increasing in magnitude as x_2 becomes less negative) although detailed agreement is lacking. Some of the disagreement between the B_1 and B_3 components could be explained by a misalignment of the magnetometer with respect to the x_2 axis (axis of the boom), but not all of the discrepancy can be described by this effect (e.g., the total field does not agree at each point). As might be expected, the largest discrepancies in the total field occur at the two points which are the farthest from the region where the analytic model was fit, those points indicated as near E-1 and E-4.

The total earth's magnetic field extracted from the data taken in this experiment (Eq. 33) is about 47,200 gamma. This is somewhat smaller

than the value of about 49,000 gamma given by Knecht [David J. Knecht, "The Geomagnetic Field (A Revision of Chapter 11, Handbook of Geophysics and Space Environments)," Air Force Cambridge Research Laboratories AFCRL-72-0570, 1972, pages 46-50] for the San Diego, California area (adjusted to 1976). The vertical component given in Eq. 33 is very close to Knecht's value of 41,500 gamma, but the horizontal component (22,500 gamma) is smaller by several thousand gamma (Knecht gives 26,100 gamma, both vertical and horizontal components adjusted to 1976). The declination angle for the field of Eq. 33 is only about 10° , compared to an expected value closer to 14° . However, the actual alignment of the coordinate system defined in figure 5 with respect to true north was not verified.

Coordinates of Measurement Point		Magnetic Field - First line is experi- mental data; Second line is analytic Model result			
x_2 (meters)	x_3 (meters)	B_1	B_2	B_3	$ B $
- 9.9	-19.6	21,470	16,080	33,090	42,597
(~E-1)		17,258	14,986	33,023	40,161
-12.9	-19.6	22,100	10,360	36,750	44,117
(~D-1)		20,399	12,067	37,001	43,941
-15.9	-19.6	23,470	8,850	37,590	45,190
(~C-1)		21,430	9,907	38,887	45,492
-21.9	-19.6	25,280	7,390	36,660	45,140
(~A-1)		21,987	7,393	40,419	46,602
-21.5	-24.2	24,810	6,910	37,120	46,179
(~A-3)		22,003	7,973	41,184	47,369
-11.5	-28.1	23,200	15,820	42,310	50,780
(~E-4)		20,686	16,340	45,015	47,889

Table A-1. Magnetic field components and total field in units of gamma as measured at six points near the NUC in January 1975, and the results of the analytic field model. The approximate locations in terms of the positions indicated in figure 1 are shown in parenthesis (Position E-4 is a few meters above position E-3). This experimental data is courtesy of Richard Ziemer of Physical Dynamics, Inc., Santa Monica, CA.

METRIC SYSTEM

BASE UNITS:

Quantity	Unit	SI Symbol	Formula
length	metre	m	...
mass	kilogram	kg	...
time	second	s	...
electric current	ampere	A	...
thermodynamic temperature	kelvin	K	...
amount of substance	mole	mol	...
luminous intensity	candela	cd	...

SUPPLEMENTARY UNITS:

plane angle	radian	rad	...
solid angle	steradian	sr	...

DERIVED UNITS:

Acceleration	metre per second squared	...	m/s
activity (of a radioactive source)	disintegration per second	...	(disintegration)/s
angular acceleration	radian per second squared	...	rad/s
angular velocity	radian per second	...	rad/s
area	square metre	...	m
density	kilogram per cubic metre	...	kg/m
electric capacitance	farad	F	A·s/V
electrical conductance	siemens	S	A/V
electric field strength	volt per metre	...	V/m
electric inductance	henry	H	V·s/A
electric potential difference	volt	V	W/A
electric resistance	ohm	...	V/A
electromotive force	volt	V	W/A
energy	joule	J	N·m
entropy	joule per kelvin	...	J/K
force	newton	N	kg·m/s
frequency	hertz	Hz	(cycle)/s
illuminance	lux	lx	lm/m
luminance	candela per square metre	...	cd/m
luminous flux	lumen	lm	cd·sr
magnetic field strength	ampere per metre	...	A/m
magnetic flux	weber	Wb	V·s
magnetic flux density	tesla	T	Wb/m
magnetomotive force	ampere	A	...
power	watt	W	J/s
pressure	pascal	Pa	N/m
quantity of electricity	coulomb	C	A·s
quantity of heat	joule	J	N·m
radiant intensity	watt per steradian	...	W/sr
specific heat	joule per kilogram-kelvin	...	J/kg·K
stress	pascal	Pa	N/m
thermal conductivity	watt per metre-kelvin	...	W/m·K
velocity	metre per second	...	m/s
viscosity, dynamic	pascal-second	...	Pa·s
viscosity, kinematic	square metre per second	...	m/s
voltage	volt	V	W/A
volume	cubic metre	...	m
wavenumber	reciprocal metre	...	(wave)/m
work	joule	J	N·m

SI PREFIXES:

Multiplication Factors	Prefix	SI Symbol
1 000 000 000 000 = 10 ¹²	tera	T
1 000 000 000 = 10 ⁹	giga	G
1 000 000 = 10 ⁶	mega	M
1 000 = 10 ³	kilo	k
100 = 10 ²	hecto*	h
10 = 10 ¹	deka*	da
0.1 = 10 ⁻¹	deci*	d
0.01 = 10 ⁻²	centi*	c
0.001 = 10 ⁻³	milli	m
0.000 001 = 10 ⁻⁶	micro	μ
0.000 000 001 = 10 ⁻⁹	nano	n
0.000 000 000 001 = 10 ⁻¹²	pico	p
0.000 000 000 000 001 = 10 ⁻¹⁵	femto	f
0.000 000 000 000 000 001 = 10 ⁻¹⁸	atto	a

* To be avoided where possible.